P. Chandran, (iD) R. Gopal, V. K. Chandrasekar, et al.

View Online   Export Citation   CrossMark

Chimera states in coupled logistic maps with additional weak nonlocal topology

P. Chandran,[1] R. Gopal,[2] (ID) V. K. Chandrasekar,[2] and N. Athavan[1] (ID)

AFFILIATIONS

[1]Department of Physics, H.H. The Rajah's College, Pudukkottai 622 001, Tamil Nadu, India
[2]Centre for Nonlinear Science & Engineering, School of Electrical & Electronics Engineering, SASTRA Deemed University, Thanjavur 613 401, Tamil Nadu, India

ABSTRACT

We demonstrate the occurrence of coexisting domains of partially coherent and incoherent patterns or simply known as chimera states in a network of globally coupled logistic maps upon addition of weak nonlocal topology. We find that the chimera states survive even after we disconnect nonlocal connections of some of the nodes in the network. Also, we show that the chimera states exist when we introduce symmetric gaps in the nonlocal coupling between predetermined nodes. We ascertain our results, for the existence of chimera states, by carrying out the recurrence quantification analysis and by computing the strength of incoherence. We extend our analysis for the case of small-world networks of coupled logistic maps and found the emergence of chimeralike states under the influence of weak nonlocal topology.

Published under license by AIP Publishing. https://doi.org/10.1063/1.5084301

Chimera state is a coexistence of coherent and incoherent domains originally believed to exist in networks of nonlocally coupled oscillators. Global and small-world networks with identical elements were since recently not the potential candidates for the exhibition of chimera states unless and otherwise perturbed suitably. Hence, we consider a network of globally coupled logistic maps and add to it a nonlocal topology of very weak coupling strength with an aim of observing chimera states. By keeping the nonlocal coupling strength very small and gradually varying the strength of global coupling, a transition, from an incoherent state to a completely synchronized state, takes place. During the transition itinerancy state, the anticipated chimera state and cluster state emerge for different global coupling strengths. If we allow some nodes to delink their own nonlocal connections, the chimera states survive as long as there is a sufficient amount of nonlocally weakly coupled nodes. Also, when we introduce a symmetric gap distribution in the nonlocal coupling between preferred nodes, the chimera states survived. For both cases, we have analyzed two different coupling radii. Quantitatively, we have studied the characteristic behavior of the existence of chimera states and other collective dynamical states using the recurrence quantification analysis, by computing the strength of incoherence and spatial correlation measure. Finally, we extend our analysis for the case of small-world networks of coupled logistic maps perturbed by weak nonlocal

couplings and demonstrate the emergence of chimeralike states as well. Here also, we have studied the extent of survival of chimera states upon delinking of nonlocal connections by the two different methods mentioned above but for two different probabilities.

I. INTRODUCTION

In recent times, a huge amount of research work has been devoted to understand the existence of chimera states in networks of identical oscillators,[1-6] which are abundant in physics, chemistry, biology, neurology, and so on. A chimera state can be defined as a spatial domain corresponding to coupled elements wherein partially coherent and partially incoherent states coexist. These states simply emerge as a hybrid state when there is a transition between completely incoherent (desynchronized) and completely coherent (synchronized) states in a nonlocally coupled system with appropriate coupling strength.[7-17] This remarkable phenomenon has been initially identified in nonlocally coupled identical phase oscillators using complex Ginzburg–Landau equations by Kuramoto and Battogtokh[18] and later in Kuramoto–Sakaguchi phase model.[19] Also, different types of systems like mechanical oscillators,[20] chemical oscillators,[21] and neuron models[22] have been known to exhibit

chimera states. Further, different types of chimera states such as frequency chimera,[16] amplitude and phase chimera,[17] amplitude mediated chimera,[3] imperfect chimera,[23] and multicluster chimera[24] have been reported in the recent literature. Earlier works focused only on networks with nonlocally coupled oscillators to show the existence of such a phenomenon.[25–43] This has created the notion that nonlocal couplings were supposed to be the key ingredients for the identification of chimera states in networks.

Recently, the authors in Refs. 44–50 have shown that the chimeralike states can even be induced in globally coupled networks. Also, several investigations have been reported in the recent past with respect to the emergence of chimeralike states in globally coupled oscillator networks.[51–53] In particular, it has already been shown that in globally as well as in locally coupled networks of oscillators, the symmetry breaking phenomenon is the primary cause for the emergence of chimeralike states from a completely coherent state.[45,46,54–56] By and large, synchronization phenomenon has been explored in networks of coupled dynamical systems, where the coupling topology can be expressed in terms of complex schemes.[57–61] However, while some of the globally coupled networks are unable to show chimera states in a pure form, several researchers have tried to add or induce heterogeneity so as to exhibit chimera states and have succeeded. Such examples include, Omelchenko *et al.* with an additional spatially modulated time-delayed coupling and nonperiodic boundaries,[44] Chandrasekar *et al.* with additional intensity dependent frequency,[47] Ko and Ermentrout with a truncated power-law distribution coupling strengths,[48] Wang and Li using weighted frequencies of heterogeneous oscillators,[49] Schmidt *et al.* with nonlinear mean-field coupling,[50] and so on.

Motivated by this, in the present work, we explore the possibility of the existence of chimera states in globally coupled networks with a meager addition of nonlocal topology which has not been done so far with regard to global networks. We find that the nonlocal topology of very weak coupling strength is enough to induce heterogeneity among the elements of the system, which, in turn, exhibits chimera states. Also, we extend the idea of adding very weak nonlocal topology to the coupled dynamical systems of small-world networks and observed the appearance of chimeralike states. In a nutshell, the above mentioned composite coupling schemes make the system concerned to show the chimera in addition to other collective dynamical states.

The structure of the paper is organized as follows: In Sec. II, we present our model and mention the quantification measures to characterize the chimera and other collective dynamical states in terms of recurrence quantification analysis and strength of incoherence. Also, we describe the mechanism for the existence of chimera states along with spatial correlation measure, a quantity used to study the spatial evolution of chimera states. Further, we illustrate, the extent of survival of chimera states under partial nonlocal disconnections by two different schemes, viz., selective removal of nonlocal connections and introduction of symmetric gaps between the nonlocally connected nodes. In Sec. III, we describe the emergence of chimera-like states in small-world networks of coupled logistic maps in the similar manner as we expressed in Sec. II. We summarize our results in Sec. IV. In Appendix A, we show the existence of chimera states in globally coupled continuous dynamical systems (Rössler oscillator) upon perturbing with weak nonlocal topology.

II. STUDY OF CHIMERA STATES IN NETWORKS OF GLOBALLY COUPLED LOGISTIC MAPS

A. Model

Generally, the interaction of dynamical elements in real-world networks can be modeled by coupled map lattices (CML). It has been found that they are very much useful in several practical situations arose in areas such as fluid dynamics,[62] hydrodynamic turbulence,[63] ecological systems,[64] logic gates and implementation of dynamics based computation,[65,66] and so on. During the last decades, several works on coupled maps have been accomplished using regular coupling scheme,[67–69] global coupling scheme,[70,71] sparse networks,[72,73] long range connections,[74,75] and nonlocal coupling scheme.[7,8] In our study, we consider CML in the form of globally coupled logistic maps with additional nonlocal topology, whose underlying dynamics has been represented by the following equation:

$$x_i^{t+1} = f(x_i^t) + \sum_{j=1}^{N} g_{ij} \left[f(x_j^t) - f(x_i^t) \right], \quad i = 1, \ldots, N. \quad (1)$$

Here, x_i are real dynamical variables, N is the total number of nodes (elements), t denotes the discrete time step, and function $f(x)$ is given by $f(x) = ax(1 - x)$ for the case of logistic map. As our investigation needs that the logistic maps are to be in the chaotic state, we fix the control parameter $a = 3.8$. The connection topology g_{ij} can be represented as

$$g_{ij} = \frac{\epsilon}{N} + \frac{\sigma}{2P} \eta_{ij}, \quad (2)$$

where ϵ and σ ($\ll 1$) denote the strength of global and nonlocal coupling, respectively. P specifies the number of nearest neighbors in both directions coupled with the ith node, and η_{ij} represents the connectivity matrix whose elements are 1 when nodes i and j are interconnected under the condition $j \leq i \pm P$ (modulo N) or 0 otherwise. The quantity $\frac{P}{N}$ denotes the coupling radius r. From Eqs. (1) and (2), one can understand that the ith node of a ring is coupled to all the other nodes of the ring and also with P number of nodes in both directions with respect to its location in the ring which are symmetric with respect to all the nodes. Hence, the spatial rotational symmetry is preserved. Moreover, the strength of each node is the same. In our numerical simulations, we take $N = 1000$ (the results have also been verified for the independent size of the system) and we choose the initial conditions of x_i^0 using the expression $x_i^0 = \sin(\frac{i\pi}{N})$.[7,8]

B. Quantification measures to characterize the chimera and other collective dynamical states

To characterize the observed dynamical states including chimera state, we use the following quantitative measures.

(i) *Recurrence quantification analysis*: For the identification of chimera states and distinguish various other dynamical states, we use the recurrence plot (RP) and calculate the recurrence rate (RR).[76,77] A point (i, j) in the recurrence plot is determined by the expression

$$RP_{i,j} = \Theta(\xi - \|x_i - x_j\|), \quad (3)$$

where x_i and x_j are the real dynamical variables of ith and jth nodes, respectively, of the network, ξ is a threshold value, $\|.\|$ denotes the

Euclidean norm, and $\Theta(.)$ is the Heaviside step function. A recurrence occurs whenever two variables x_i and x_j have roughly the same value such that the argument of Θ is positive. In other words, the recurrence point (i, j) in the plot corresponds to the unit value of Θ. The recurrence rate is the density of recurrence points given by

$$RR(\xi) = \frac{1}{N^2} \sum_{i=1}^{N} \sum_{j=1}^{N} RP_{i,j}(\xi). \qquad (4)$$

(ii) *Strength of incoherence* (S): Another important quantity to confirm the existence of chimera states and various dynamical states is the strength of incoherence. This can be calculated using the expression[10]

$$S = 1 - \frac{1}{M} \sum_{m=1}^{M} s_m, \qquad s_m = \Theta(\delta - D(m)), \qquad (5)$$

where $\Theta(.)$ is the Heaviside step function, and δ is a predefined threshold and chosen to be a certain percentage value of the difference between $x_{i,max}$ and $x_{i,min}$. M is the number of (even) bins of equal length $n = N/M$, where N is the total number of nodes. The quantity $D(m)$, which is the local standard deviation, is given by

$$D(m) = \left\langle \sqrt{\frac{1}{n} \sum_{j=n(m-1)+1}^{mn} [z_j - \langle z_m \rangle]^2} \right\rangle_t, \qquad m = 1, 2, \ldots, M, \qquad (6)$$

where $z_i = x_i - x_{i+1}$, $i = 1, 2, \ldots, N$, $\langle z_m \rangle = \frac{1}{n} \sum_{j=n(m-1)+1}^{mn} z_j$, and $\langle . \rangle_t$ represents the time average. The above quantity $D(m)$ is calculated for every successive n number of nodes. When $D(m)$ is less than δ, the value of $s_m = 1$, otherwise it is 0.

C. Absence and presence of nonlocal topology (σ)

To begin with, by iterating the system (1) without nonlocal topology ($\sigma = 0$), we observe that the system transits from an incoherent state to a completely synchronized state only through the itinerancy state as we increase the global coupling strength gradually. In Fig. 1, we have presented the snapshots alongside their respective spatiotemporal plots and recurrence plots for various values of global coupling strength ϵ. For a small value of global coupling strength $\epsilon = 0.10$, we observe the incoherent state where the values of x_i spread out considerably, which can be seen in Figs. 1(a) and 1(d). The corresponding recurrence plot in Fig. 1(g) shows a diagonal line, which is clearly seen, and the plot does not have any specific structure. The points are randomly distributed. When we increase the global coupling strength to $\epsilon = 0.29$, we find that the instantaneous states of the maps got distributed between low and high dimensional states (both the states are periodic in time in our case) leaving most of the nodes incoherent. This phenomenon is called itinerancy and the corresponding state is called itinerancy state. (Since only the chaotic itinerancy has been defined for the case of chaotic higher dimensional state in the literature,[7,78] we just mention our observation as itinerancy state.) They have been depicted in Figs. 1(b) and 1(e). Figure 1(h) represents the recurrence plot for the itinerancy state whose spatial structure has black boxes of different sizes with some white patches. Upon increasing the global coupling strength further to $\epsilon = 0.40$, the coupled maps are completely synchronized in
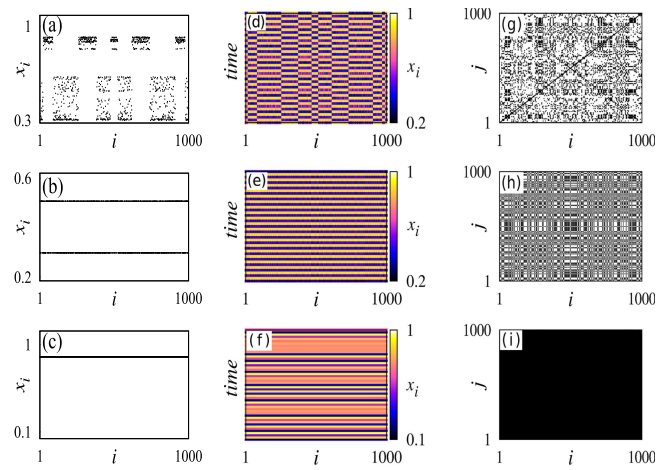

FIG. 1. Snapshots of the dynamical states of the system (1) without nonlocal topology ($\sigma = 0$). (a) represents the incoherent state for $\epsilon = 0.10$, (b) shows the itinerancy state for $\epsilon = 0.29$ and (c) depicts the completely synchronized state for $\epsilon = 0.40$. Further, (d)–(f) and (g)–(i) represent the corresponding spatiotemporal plots and recurrence plots for (a)–(c).

a periodic orbit as shown in Figs. 1(c) and 1(f). The corresponding recurrence plot is entirely black due to regular spatial behavior as shown in Fig. 1(i).

Now, we introduce the nonlocal topology with minimal coupling strength by keeping the value of σ at 0.05 and iterate Eq. (1). Interestingly, we observe the transition from the incoherent state to the completely synchronized state via the itinerancy state and the most exciting chimera state as we vary the global coupling strength ϵ. In Fig. 2, we present the snapshots and the corresponding recurrence plots for various values of global coupling strength ϵ with coupling radius $r = 0.2$. For a small value of ϵ, that is, $\epsilon = 0.08$, we obtain the incoherent state as shown in Fig. 2(a). Figure 2(e) shows the corresponding recurrence plot that has a diagonal line in addition to the random distribution of points. When we increase the value of ϵ to 0.24, we find the emergence of the itinerancy state as shown in Fig. 2(b) and the corresponding recurrence plot in Fig. 2(f). Further increase in ϵ, say, $\epsilon = 0.27$, induces the system to have, simultaneously, the coherent and incoherent states which one can term it as, the most intriguing, chimera states,[7,8] whose pictorial representation is depicted in Fig. 2(c). This state is similar to the one observed in Figs. 2(c) and (d) of Ref. 7. The respective recurrence plot has large islands (white portions) due to the presence of more number of incoherent states, which is clearly illustrated in Fig. 2(g). Finally, we observe the completely synchronized state for $\epsilon = 0.35$ that is shown in Fig. 2(d). The corresponding recurrence plot is completely black due to the regular spatial structure as shown in Fig. 2(h).

In order to confirm and quantify the existence of chimera states and other collective dynamical states for the model mentioned in Eq. (1), we have calculated the strength of incoherence using Eq. (5) and computed the recurrence rate using Eq. (4). We have plotted the strength of incoherence (S) and recurrence rate (RR) in Fig. 3 as a function of global coupling strength ϵ for the cases without and with
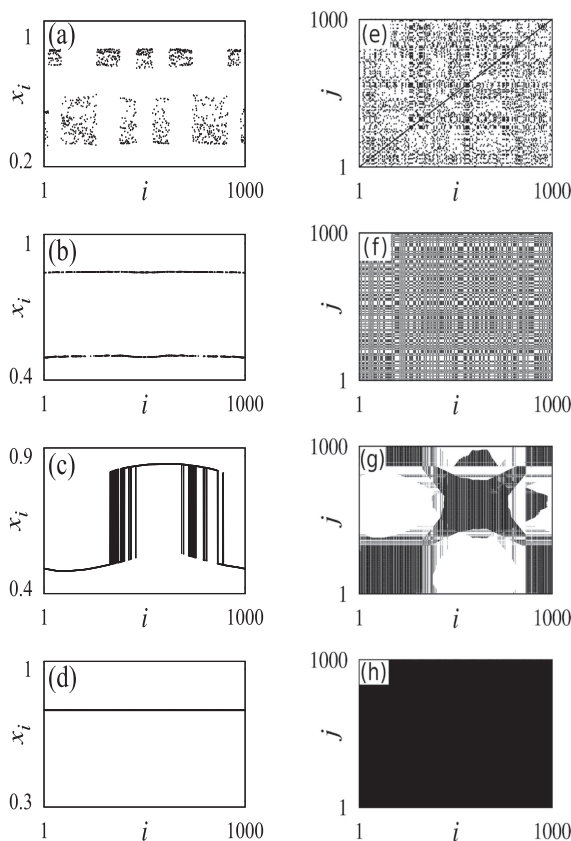
FIG. 2. Snapshots (left column) and recurrence plots (right column) of the system (1) for $\sigma = 0.05$ and $r = 0.2$. (a) and (e) show incoherent states for $\epsilon = 0.08$, (b) and (f) represent itinerancy states for $\epsilon = 0.24$, (c) and (g) show chimera states for $\epsilon = 0.27$, (d) and (h) represent completely synchronized states for $\epsilon = 0.35$.

FIG. 3. Plots of strength of incoherence (S) and recurrence rate (RR) as a function of global coupling strength ϵ for system (1) with $r = 0.2$. (a) for $\sigma = 0$, (b) for $\sigma = 0.05$. Here, incoherent state, itinerancy state, chimera state, cluster state, and completely synchronized state are mentioned as IC, IT, CH, CL, and CS, respectively.

nonlocal coupling strength σ. For $\sigma = 0$, we observe the transition from the incoherent state to the completely synchronized state via the itinerancy state as the global coupling strength ϵ is increased as shown in Fig. 3(a). Here, the value of S is unity and the value of RR is very close to 0 both of which represent the incoherent state in the range of $\epsilon \in (0, 0.15)$. Itinerancy state exists in the range $\epsilon \in (0.15, 0.35)$, with $S = 0.95$ and RR is little over than that of the incoherent state. Beyond $\epsilon = 0.35$, S attains a null value while RR has a constant larger value than that for the itinerancy state both of which confirm the existence of the completely synchronized state. No chimera state exists in this case as the system jumps down to the completely synchronized state immediately after the itinerancy state even for a small increase in ϵ above 0.35. Now, we introduce a weak nonlocal coupling strength by setting $\sigma = 0.05$. The system makes the transition from the incoherent state to the itinerancy state, then to the chimera state, next to the cluster state and finally to the completely synchronized state as the global coupling strength ϵ is increased from 0 to 0.4, which are shown in Fig. 3(b). In this case, only due to the presence of nonlocal topology with weak coupling strength, we could
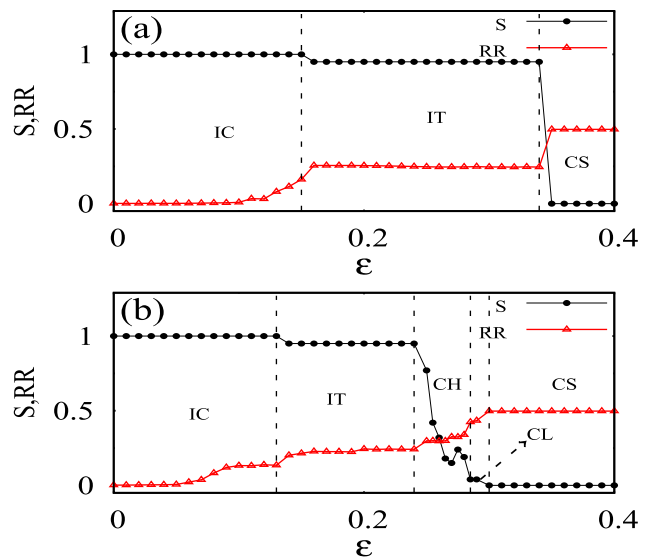
observe the chimera state in the range of $\epsilon \in (0.25, 0.28)$. This is evident from the obtained values of S ($0.95 < S < 0.1$) which seem to fall down and the corresponding RR values smoothly rise up for the range of $\epsilon \in (0.25, 0.28)$. Further, the system goes to the completely synchronized state as we increase ϵ beyond 0.30, gradually. We extend the above study also for the case of globally coupled Rössler oscillators perturbed with weak nonlocal topology and their results are given in Appendix A.

To determine the behavior of individual elements of the model, we plot bifurcation diagrams for the entire regime of ϵ considered for our analysis. We show in Figs. 4(a) and 4(b) the bifurcation diagrams of the 457th element for the cases $\sigma = 0$ and $\sigma = 0.05$, respectively. The element is incoherent when the chimera state appears. The discontinuous "broken" lines preceeding the chaotic windows are evidence that this unit presents the coexistence of periodic regimes, and as such each existing regime has its own spatial basin of attraction,[79] a condition required for chimera. From the bifurcation diagram, periodic orbits appear for the itinerancy state, and noncoexisting chaotic states appear for nonchimera states (either maps are fully desynchronous or fully synchronous).

D. Mechanism behind the existence of chimera states

We explain the mechanism of chimera states using the quantity $|z_i|$, where z_i is defined in Eq. (6). $|z_i|$ is 0 when ith and $(i + 1)$th elements are coherent and nonzero when they are incoherent. We mention the probability of getting a particular value of $|z_i|$ as $p(|z_i|)$.

When the elements of the network are uncoupled ($\epsilon = 0$; $\sigma = 0$) $|z_i|$ is random and the distribution of $p(|z_i|)$ is flat due to the chaotic behavior of the elements. If we increase the value of global
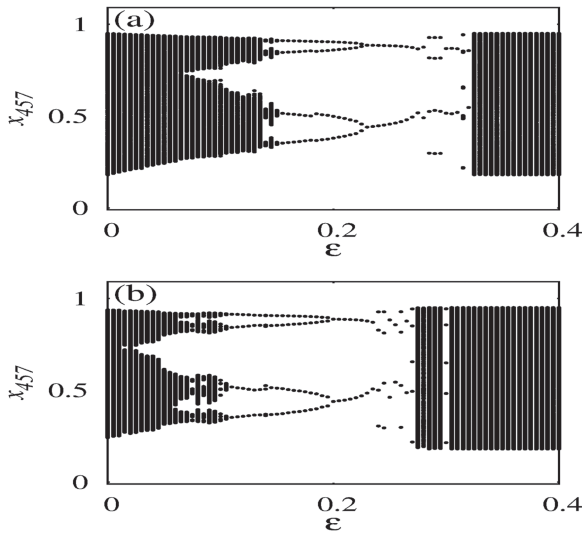
FIG. 4. Bifurcation diagrams for the element x_{457} as a function of global coupling strength ϵ of the system (1) with $r = 0.2$. (a) for $\sigma = 0$, (b) for $\sigma = 0.05$. At each value of ϵ, 1000 iterates are plotted after initial transients.

coupling strength ϵ gradually and keep around 0.2, the elements of the network gradually lose their chaotic behavior and try to settle down to a particular kind of oscillation due to the periodic nature of the maps for $\epsilon \approx 0.2$ as can be seen from the bifurcation diagram (Fig. 4). The elements may be in either of the two equally probable states. Therefore, the value of $|z_i|$ is unique for all incoherent elements. This corresponds to the itinerancy state where most of the

elements are incoherent with respect to their neighbors except a very few. This is depicted in Figs. 5(a) and 5(b). Now, if we apply nonlocal topology of small coupling strength with a suitable coupling radius, each element tries to influence its immediate neighbors on either sides and, thus, makes them to mimic its state. This process increases the number of coherent elements in the network. The probability $p(|z_i|)$ for $|z_i| = 0$ is larger. A further increase in the value of coupling radius results in a large number of coherent states. Hence, both the coherent and incoherent domains coexist that signifies the existence of chimera states. In Figs. 5(c)–5(f), we present the plots of chimera states for $r = 0.18$ and $r = 0.33$, respectively. Finally, for large coupling radius, almost all the elements become coherent except some having nonzero $|z_i|$ which makes a few discontinuities in the profile. This state corresponds to a cluster state and depicted in Fig. 5(h).

As the snapshots only depict the chimera profiles at certain instants of time, for the purpose of analyzing the spatial evolutions of the respective spatial domains of coherent and incoherent elements, we quantify the spatial coherence by computing the spatial correlation measure $(C_{sp})^{80,81}$ which is given by

$$C_{sp} = \left\langle \frac{1}{N} \sum_{i=1}^{N} h(|z_i|) \right\rangle_t, \tag{7}$$

where the function $h(|z_i|)$ is given as

$$h(|z_i|) = \begin{cases} 1 & \text{if } |z_i| \leq \vartheta, \\ 0 & \text{otherwise.} \end{cases}$$

Here, ϑ is a threshold value that can be fixed as some percentage of the maximum value of $|z_i|$ possessed by the system. Therefore, the null value of C_{sp} resembles the incoherent state, whereas the unit value of C_{sp} represents the completely synchronized state. However,
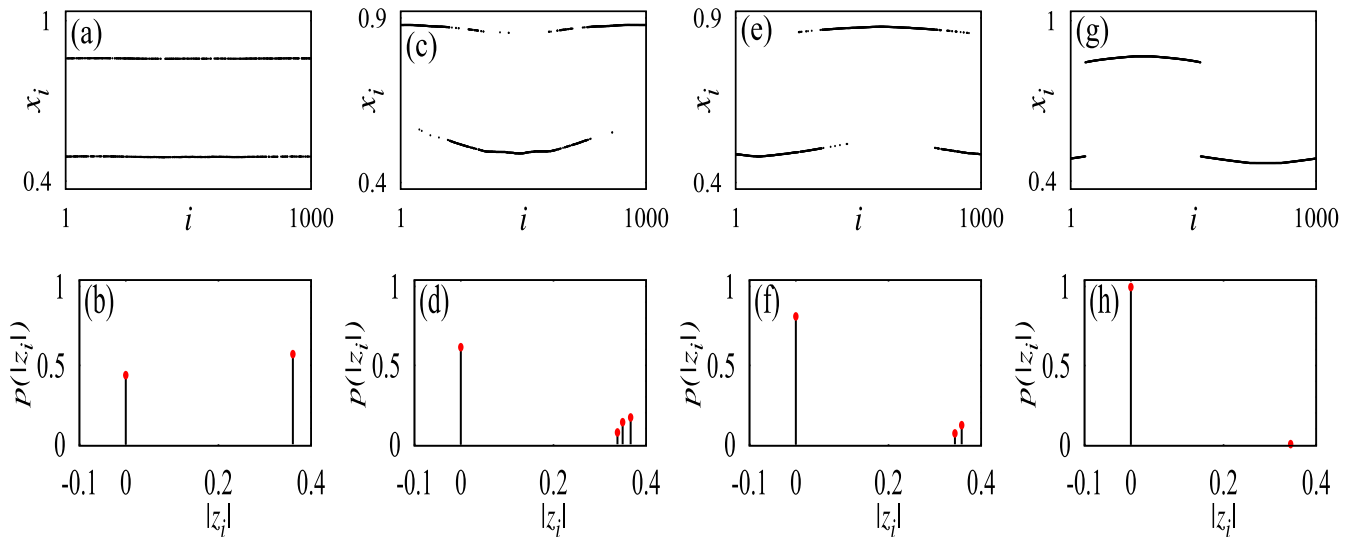

FIG. 5. Snapshots of x_i (top row) and probability distributions of $p(|z_i|)$ (bottom row) of the system (1) for various values of coupling radius r with $\epsilon = 0.27$ and $\sigma = 0.05$. (a) and (b) show itinerancy states for $r = 0.05$, (c), (d) and (e), (f) mention chimera states for $r = 0.18$ and $r = 0.33$, respectively, (g) and (h) represent cluster states for $r = 0.42$.

the intermediate values of C_{sp} manifest the itinerancy, chimera, and cluster states. In Fig. 6(a), we show the spatial correlation measure C_{sp} as a function of coupling radius r by keeping the values of other parameters as the same as in Fig. 5. In the lower coupling radius range, that is, $r \in (0.01, 0.07)$, the value of C_{sp} seems to increase gradually from a smaller value. This region corresponds to the itinerancy state which contains a large number of incoherent elements and a small number of coherent elements. The system possesses the chimera state from the itinerancy state in the range of $r \in (0.07, 0.39)$. In this region, most of the maps evolve in the coherent state, while least of the maps evolve in the incoherent state. Therefore, the value of C_{sp} is higher than that of the previous state. Cluster states appear with more number of coherent states when the value of the coupling radius r lies within the range $r \in (0.39, 0.45)$, where the value of C_{sp} is slightly under unity. For $r > 0.45$, the unit value of C_{sp} indicates the emergence of the completely synchronized state. Similarly, the above dynamical transitions are depicted in Fig. 6(b) but for C_{sp} as a function of global coupling strength ϵ.

E. Removal of selective nonlocal connections

In Sec. II C, we have discussed the existence of chimera states in networks of globally coupled maps by adding nonlocal topology with weak coupling strength. Now, in order to check the extent of the survival of the chimera states, we make N_f nodes out of N nodes to delink their own nonlocal connections as illustrated schematically in Fig. 7. This can be numerically done by making the elements of connectivity matrix $\eta_{ij} = 0$ for $i > N_f$ for all allowed values of $j \leq i \pm P$ (modulo N) in Eq. (1). The nonlocal disconnection ratio R is represented as

$$R = \frac{N_f}{N}, \tag{8}$$

where N_f is the number of nodes freed from nonlocal connections (NLC) and N is the total number of nodes. We observe that the chimera states still emerge when we disconnect the nonlocal connections (in steps of 10) of some of the nodes. To illustrate the results, we have plotted the strength of incoherence (S) as a function of nonlocal disconnection ratio (R) for two different coupling radius r with $\epsilon = 0.27$ and $\sigma = 0.05$ in Fig. 8(a) and for two different global coupling strength ϵ with fixed coupling radius $r = 0.2$ and $\sigma = 0.05$ in Fig. 8(b). By keeping the value of $r = 0.15$, we find that the system shows chimera states as long as we keep R less than 0.53. This clearly
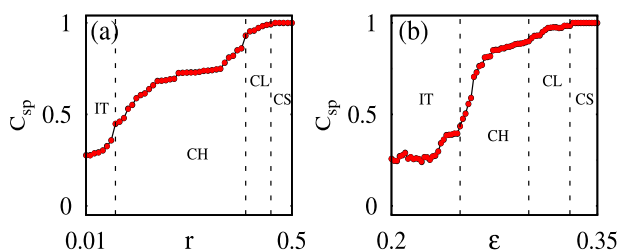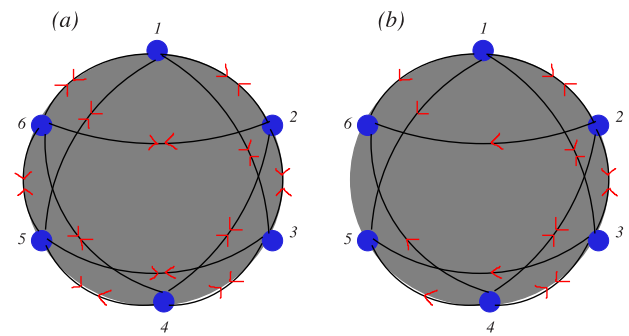

FIG. 7. Schematic representation of the selective removal of nonlocal connections: For the purpose of illustration, we have taken $N = 6$ and $P = 2$. Gray color denotes the sea of global connections, and black lines represent the weak nonlocal connections. The red arrow indicates the direction of nonlocal connections. (a) Before delinking of nonlocal connections, (b) after delinking of nonlocal connections correspond to nodes 5 and 6 ($N_f = 2$).

denotes that the chimera states can still be found in the system even for the disconnections of NLC up to 530 nodes from the nonlocal topology out of 1000 nodes. In other words, the concerned system needs at least 47% nonlocal connections to show the chimera states for $r = 0.15$, $\epsilon = 0.27$, and $\sigma = 0.05$, which is shown in Fig. 8(a) (represented by black dots). For $R > 0.53$, the system attains itinerancy states. For $r = 0.25$, we can observe the chimera states for the range of $0 \leq R \leq 0.56$. Further for $R > 0.56$, the system attains itinerancy states. For $\epsilon = 0.25$ and 0.28, we observe that the system exhibits chimera states in the range of $0 \leq R \leq 0.54$. For $R > 0.54$, the system transits into itinerancy states. Hence, we conclude that almost half of the total nodes need to be nonlocally connected in addition to the global connectivity for the observation of chimera states in the system concerned.

The spatiotemporal plots for two different values of R, that is, $R = 0.2$ and $R = 0.27$, are shown in Figs. 8(c) and 8(d), respectively, with $r = 0.2$, $\epsilon = 0.28$, and $\sigma = 0.05$. From the plots, one can understand the spatiotemporal evolution of chimera states when selective nodes are freed from nonlocal topology. In Ref. 73, the authors have investigated that a minimal connectivity (i.e., for sparse networks) is enough to sustain a collective dynamics in random networks. Similarly, we have also shown that our system exhibits chimera states with respect to minimal (or partial) nonlocal connectivity.

F. Introduction of symmetric gap distribution

Here, we discuss the existence of chimera states in system (1) by introducing symmetric gap distribution in the nonlocal coupling between preferred nodes and their neighbors. Symmetric gaps have been introduced in the nonlocal coupling on both sides with reference to each node where each node was coupled initially with a finite number of $2P \leq N$ nodes. P is the number of nearest neighbors in each side. The gaps are arranged symmetrically on the left and on the right of each node. If G_L and G_R are the sizes of gaps situated to the left and to the right of a node, respectively, then it follows

FIG. 6. (a) Plot of spatial correlation measure C_{sp} as a function of coupling radius r with $\epsilon = 0.27$ and $\sigma = 0.05$, (b) plot of spatial correlation measure C_{sp} vs global coupling strength ϵ with $r = 0.1$ and $\sigma = 0.05$.

FIG. 9. The strength of incoherence (S) is plotted against symmetric gaps (G) for system (1) for two different coupling radius r. The parameter values are $P_2 = 50$, $P_1 = P - P_2 - G$, $\epsilon = 0.27$, and $\sigma = 0.05$.
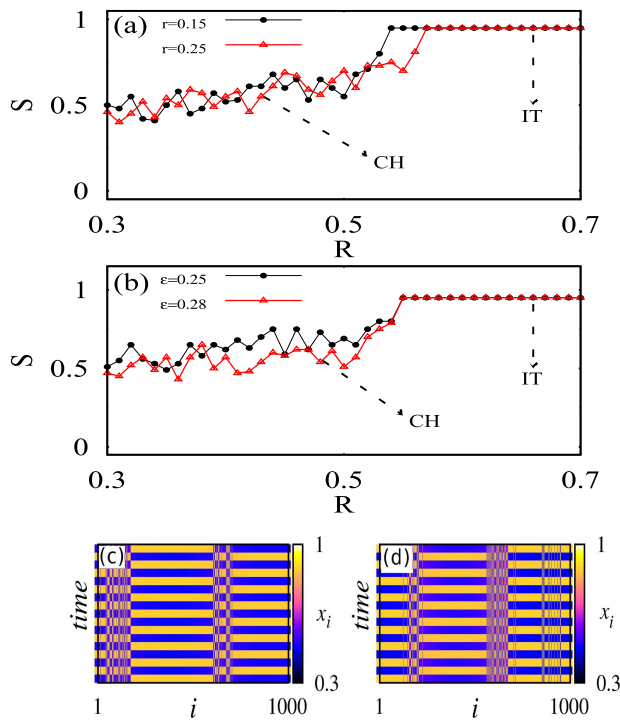

FIG. 8. Strength of incoherence (S) vs nonlocal disconnection ratio (R) for system (1). (a) Plots for two different values of coupling radius r with $\sigma = 0.05$ and $\epsilon = 0.27$, (b) plots for two different global coupling strength ϵ with fixed coupling radius $r = 0.2$ and $\sigma = 0.05$. (c) and (d) denote the spatiotemporal plots for $R = 0.2$ and $R = 0.27$, respectively. The other parameter values are $r = 0.2$, $\epsilon = 0.28$, and $\sigma = 0.05$.

that $G_L + G_R + 2P \leq N$. For the symmetric case ($G_L = G_R = G$), the connectivity matrix (η_{kl}), $k, l = 1, \ldots, N$, is given by[15]

$$\eta_{kl} = \begin{cases} 1 & \text{if } k - P_1 < l < k + P_1, \\ & \text{or } k + P_1 + G < l < k + P_1 + G + P_2, \\ & \text{or } k - P_1 - G - P_2 < l < k - P_1 - G, \\ 0 & \text{otherwise,} \end{cases}$$

where all indices are taken modulo N. Here, P_1 represents the number of nearest neighbors prior to the gap and P_2 denotes the number of nearest neighbors beyond the gap. Each node will have $P(= P_1 + P_2)$ number of nonlocal connections symmetrically placed to both its left and right sides with a number of nodes in the gap equal to $G(= G_L = G_R)$, which is also symmetrically placed around it. Hence, the total number of nonlocal connections remains $2P$. In principle, one can introduce any number of symmetric gaps on the left and on the right sides of each node in a similar way subject to the condition $G_L + G_R + 2P \leq N$.

In Fig. 9, we have depicted the strength of incoherence (S) as a function of symmetric gaps (G) for two different coupling radius r with $\epsilon = 0.27$ and $\sigma = 0.05$. For $r = 0.15$, we observe that the chimera states appear for the gap size $G \leq 55$. By increasing the gap size G further, that is, for $G > 55$, the coupled
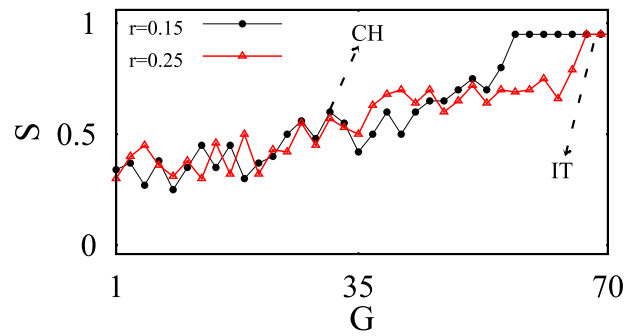
maps transit to itinerancy states. For $r = 0.25$, we find the occurrence of chimera states for the range of gap size $1 \leq G \leq 65$. For $G > 65$, the system attains itinerancy states. Though the nonlocal topology seems to be an essential ingredient for the existence of chimera states, we have demonstrated, by the methods mentioned in this and Secs. II A–II F that all the nodes need not have nonlocal connections. In other words, the partial nonlocal topology with weak coupling strength is sufficient to induce the chimera states.

G. Two parameter phase diagram

In order to analyze the global picture of the system (1) under the influence of nonlocal topology with weak coupling strength, we have plotted the two parameter phase diagram in the parametric space (ϵ, σ) in Fig. 10(a) for the fixed coupling radius $r = 0.2$. In Fig. 10(a), we show that the system is initially, for low range of ϵ (and for all values of σ), exhibiting incoherent states. By increasing the ϵ value, the system attains itinerancy states for a range of ϵ values for a given nonlocal coupling strength σ value. Upon increasing the ϵ value beyond the value correspond to itinerancy states, the system first exhibit cluster states and completely synchronized states thereafter. For $\sigma \geq 0.006$, the system transits from incoherent states to completely synchronized states via itinerancy states, chimera states and cluster states as a function of global coupling strength ϵ. Interestingly, we have brought out the existence of chimera states by the inclusion of very weak nonlocal coupling strength in the range $\sigma \geq 0.006$. Thus, we conclude that an additional nonlocal topology of very small coupling strength is enough to trigger out the chimera states in globally coupled maps.

In Fig. 10(b), we show the two parameter phase diagram for the global coupling strength $\epsilon \in (0, 0.4)$ vs the coupling radius $r \in (0.01, 0.49)$ of the system (1) with $\sigma = 0.05$. We have used the same symbols and colors as in Fig. 10(a) to indicate the different dynamical states. Here, we observe that chimera states occur only for $r \in (0.01, 0.40)$ and ceases to exist for $r \in (0.40, 0.49)$ as we vary the global coupling strength ϵ.
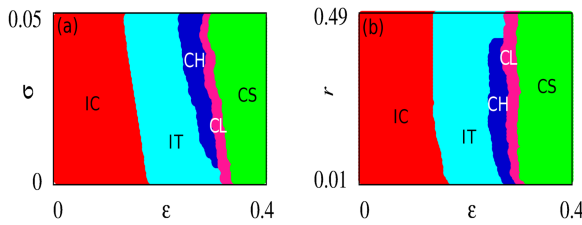
FIG. 10. Phase diagrams for the system represented in (1). (a) denotes the phase diagram in the (ϵ, σ) parametric space for fixed coupling radius $r = 0.2$. (b) depicts the phase diagram in the (ϵ, r) parametric space for $\sigma = 0.05$. IC denotes the incoherent state region, IT shows the itinerancy state region, CH depicts the chimera state region, CL is for the cluster state region, and CS represents the completely synchronized state region.

FIG. 11. Strength of incoherence (S) as a function of coupling strength μ for small-world networks of coupled maps in the absence and presence of nonlocal coupling strength σ. Here, incoherent state, itinerancy state, chimeralike state and completely synchronized state are mentioned as IC, IT, CH, and CS, respectively. The parameter values are $r = 0.2$ and $p = 0.05$.

III. STUDY OF CHIMERALIKE STATES IN SMALL-WORLD NETWORKS OF COUPLED LOGISTIC MAPS

In Sec. II, we have explored the occurrence of chimera states in networks of globally coupled logistic maps under the influence of nonlocal topology with weak coupling strength. Here, we investigate how the weak nonlocal coupling strength sparks up the emergence of chimeralike states in small-world networks as well. For our study, we choose the Newman-Watts (NW) small-world topology.[82,83] The NW small-world topology is constructed as follows: Starting with N nodes arranged in a regular ring network, each node will be connected to its nearest neighbors. Then, by randomly adding each new link of the network with probability p. The probability p is given as $p = \frac{2n_e}{N(N-1)}$, where n_e is the number of shortcuts added. The total number of possible shortcuts is $\frac{N(N-1)}{2}$. When $p = 0$, the network is simply a nearest neighbor coupled network while a globally coupled network refers to $p = 1$. For intermediate p values, that is, for $0 < p < 1$, the constructed network shows small-world features. In system (1), we just replace the global coupling component ($\frac{\epsilon}{N}$) with small-world coupling component ($\frac{\mu}{k_i} c_{ij}$), where c_{ij} represents the small-world connectivity matrix whose elements are 1 when nodes i and j are connected, subjected to probability p, or 0 otherwise and μ denotes the strength of small-world coupling. The degree k_i of node i is the number of its neighbors. The network of logistic maps so connected does not show chimeralike states without nonlocal topology. Hence, we try to add a nonlocal topology with weak coupling strength in order to induce the chimeralike states in the system (1).

Now, we identify the occurrence of chimeralike states and other dynamical states by computing the strength of incoherence. In Fig. 11, we have plotted the strength of incoherence (S) as a function of coupling strength μ in the absence and presence of nonlocal coupling strength σ. For $\sigma = 0$, we find that the coupled maps take the transition from the incoherent state to the completely synchronized state via the itinerancy state by increasing the coupling strength μ as depicted in Fig. 11 (represented by black dots). Here, the unit value of S indicates the incoherent state in the range of $\mu \in (0, 0.18)$. In the range of $\mu \in (0.18, 0.34)$, the value of $S = 0.95$ which represents the itinerancy state. Beyond $\mu = 0.34$, the value of S is 0 which confirms the existence of the completely synchronized state. Here, we
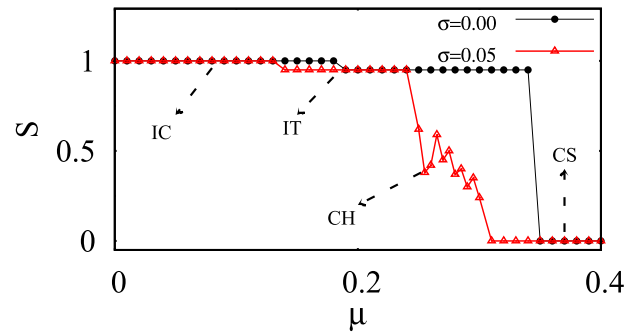
observe that no chimeralike state occurs. Next, when we introduce weak nonlocal coupling strength $\sigma = 0.05$, the coupled maps transit from the incoherent state to the completely synchronized state through the itinerancy state and chimeralike state by increasing the coupling strength μ as shown in Fig. 11 (represented by red triangles). The values of S in Fig. 11 for $\sigma = 0.05$ which fluctuate between 0 and 0.95 for the range of $\mu \in (0.25, 0.30)$ elucidate the existence of chimeralike states in the system.

For this case also, we intend to test whether the system admits chimeralike states even when we break the NLC of a certain number of nodes. For this purpose, we carry out similar analyses mentioned in Secs. II E and II F. In Fig. 12(a), we have plotted the strength of incoherence (S) as a function of nonlocal disconnection ratio (R) for two different probability p with coupling radius $r = 0.2$, $\sigma = 0.05$, and $\mu = 0.27$. We show that for $p = 0.05$, the system exhibits chimeralike states even we delink the NLC upto $R \leq 0.54$. Further disconnection of NLC beyond $R > 0.54$, makes the coupled maps to attain itinerancy states. For $p = 0.08$, we observe that the chimeralike states exist for $0 \leq R \leq 0.57$ while for $R > 0.57$ the behavior of chimera loses its stability and the states change into itinerancy states. Here also we have shown that the chimeralike states exist even after delinking certain NLC.

Further, we also identify that the system shows chimeralike states by introducing symmetric gap distribution in the nonlocal coupling between each node and its neighbors. Figure 12(b) shows the strength of incoherence (S) as a function of symmetric gaps (G) for two different probability p. For $p = 0.05$, the system shows chimeralike states in the range of gap size $1 \leq G \leq 41$. Upon further increase of the gap size, that is, for $G > 41$, the coupled maps lose their stability and then transit to itinerancy states. For $p = 0.08$, by increasing the gap size upto $G \leq 49$, we observe that the system shows chimeralike states. After the gap size $G > 49$, the system attains itinerancy states. Thus, we generalize the fact that partial nonlocal topology with weak coupling strength is sufficient to exhibit chimeralike states in networks formed using other coupling schemes. The authors in Ref. 15 have tried to introduce additional shortcut linkages between randomly selected nodes of nonlocally coupled FitzHugh-Nagumo Ł
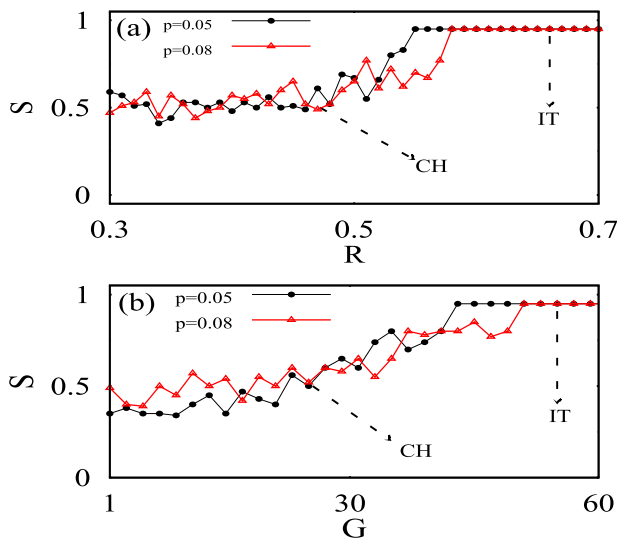
FIG. 12. (a) Plots of strength of incoherence (S) as a function of nonlocal disconnection ratio (R) for two different values of p, (b) Plots of strength of incoherence (S) as a function of symmetric gaps (G) for two different values of p. The other parameter values are $P_2 = 50, P_1 = P - P_2 - G, r = 0.2, \sigma = 0.05$, and $\mu = 0.27$.

oscillators and have reported that their topology resembles the small-world features. With a strong nonlocal coupling strength, they have shown the robustness of chimera states. However, we have demonstrated that in an actual small-world network by the inclusion of additional nonlocal topology with very small coupling strength, one can induce the chimeralike states.

IV. CONCLUSION

In this study, we have shown that the introduction of weak nonlocal topology can induce the occurrence of chimera states in networks of globally coupled logistic maps. We have illustrated the existence of chimera states and other collective dynamical states using the recurrence quantification analysis, strength of incoherence, and spatial correlation measure. We have described the mechanism through which the chimera states exist. In addition to this, we have also established that only partial nonlocal topology is enough to induce chimera states by the methods of selective delinking and symmetric gap distribution. Precisely, only certain nodes need to be perturbed with nonlocal connections of very small strength, while the other nodes remain unperturbed. In addition, we have also shown that the network with Rössler oscillators can exhibit chimera states when nonlocally perturbed. In a nutshell, we have induced heterogeneity so as to show chimera states using a composite coupling scheme among identical elements of the concerned network.

Further, we have extended our study along the same line for the case of small-world networks of coupled logistic maps perturbed with weak nonlocal topology. This suggests that partial nonlocal topology of weak coupling strength could potentially allow other types of networks to possess chimera states. Thus, the novelty of

our work was to show that the addition of weak couplings promotes the onset of chimera. Our results throw much light on areas like neuronal dynamics wherein chimeralike states play a crucial role in the diagnosis of normal functioning of brain activities (neuronal) during infections.[84–86] The phenomenon of onset and offset of chimera states in networks may be used as logical states (switching) for computational purpose.[65,66]

APPENDIX: STUDY OF CHIMERA STATES IN NETWORKS OF GLOBALLY COUPLED RÖSSLER OSCILLATORS

In order to find the existence of chimera states in globally coupled continuous dynamical systems, we replace the logistic maps with Rössler oscillators whose underlying dynamics is governed by the following set of equations:

$$\dot{u}_i = -v_i - w_i + \sum_{j=1}^{N} g_{ij} (u_j - u_i),$$

$$\dot{v}_i = u_i + \alpha v_i,$$

$$\dot{w}_i = \beta + w_i(u_i - \gamma),$$

where $i = 1, 2, \ldots, N$ and N is the total number of oscillators. The system parameters are chosen as $\alpha = 0.42$, $\beta = 2$, and $\gamma = 4$ so as to make the uncoupled oscillators to exhibit chaotic behavior.
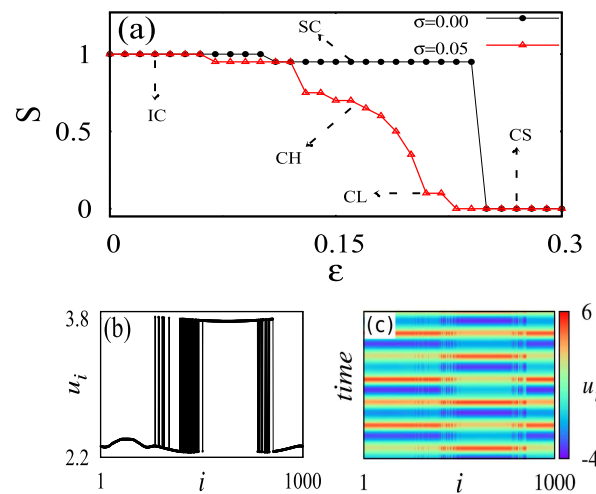

FIG. 13. (a) Plot of strength of incoherence (S) as a function of global coupling strength ϵ for globally coupled Rössler oscillators without and with nonlocal coupling strength σ. Here, SC denotes the spatial chaos state and the other dynamical states are the same as mentioned in Fig. 3. (b) and (c) are the snapshot and spatiotemporal plot, respectively, which depict the chimera state for $r = 0.25$, $\epsilon = 0.14$, and $\sigma = 0.05$ with respect to the coupled Rössler system.

The coupling topology g_{ij} is the same as in Eq. (2). The strength of incoherence (S) is depicted in Fig. 13(a) as a function of global coupling strength ϵ in the absence and presence of nonlocal coupling strength σ. For $\sigma = 0$, we observe that the oscillators transit from the incoherent state to the completely synchronized state via the spatial chaos state (similar to the itinerancy state for discrete systems) as we increase the value of ϵ. The value of S is unity in the range of $\epsilon \in (0, 0.10)$ indicating that the oscillators evolve independently. The value of S is close to unity in the range of $\epsilon \in (0.10, 0.24)$, which represents the spatial chaos state. This state is similar to the one depicted in Fig. 9(d) of Ref. 8, where the two coherent regimes split into lower and upper branches interspersed by an incoherent regime. All the oscillators evolve synchronously for $\epsilon > 0.24$, which has been confirmed by the null values of S. For $\sigma = 0.05$, as we increase the value of ϵ gradually, the oscillators make the transition from the incoherent state to the completely synchronized state via spatial chaos, chimera, and cluster states. In the range of $\epsilon \in (0.13, 0.20)$, the intermediate values of S between 0.1 and 0.95 confirm the existence of the chimera state in the system. The existence of the chimera state is shown in Fig. 13(b) for $r = 0.25$, $\epsilon = 0.14$, and $\sigma = 0.05$. The respective spatiotemporal plot shows the coexistence of coherent and incoherent patterns as given in Fig. 13(c).

REFERENCES

[1] D. M. Abrams and S. H. Strogatz, Phys. Rev. Lett. **93**, 174102 (2004).
[2] D. M. Abrams and S. H. Strogatz, Int. J. Bifurc. Chaos **16**(1), 21 (2006).
[3] G. C. Sethia, A. Sen, and G. L. Johnston, Phys. Rev. E **88**, 042917 (2013).
[4] S. Nkomo, M. R. Tinsley, and K. Showalter, Phys. Rev. Lett. **110**, 244102 (2013).
[5] O. E. Omelchenko, M. Wolfrum, and Y. L. Maistrenko, Phys. Rev. E **81**, 065201(R) (2010).
[6] A. Mishra, C. Hens, M. Bose, P. K. Roy, and S. K. Dana, Phys. Rev. E **92**, 062920 (2015).
[7] I. Omelchenko, Y. Maistrenko, P. Hövel, and E. Schöll, Phys. Rev. Lett. **106**, 234102 (2011).
[8] I. Omelchenko, B. Riemenschneider, P. Hövel, Y. Maistrenko, and E. Schöll, Phys. Rev. E **85**, 026212 (2012).
[9] N. I. Semenova, G. I. Strelkova, V. S. Anishchenko, and A. Zakharova, Chaos **27**, 061102 (2017).
[10] R. Gopal, V. K. Chandrasekar, A. Venkatesan, and M. Lakshmanan, Phys. Rev. E **89**, 052914 (2014).
[11] A. Maksimenko, V. Makarov, K. Bera, D. Ghosh, K. Dana, V. Goremyko, S. Frolov, A. Koronovskii, and E. Hramov, Phys. Rev. E **94**, 052205 (2016).
[12] E. Vadivasova, I. Strelkova, A. Bogomolov, and S. Anishchenko, Chaos **26**, 093108 (2016).
[13] I. Omelchenko, A. Zakharova, P. Hövel, J. Siebert, and E. Schöll, Chaos **25**, 083104 (2015).
[14] N. Semenova, A. Zakharova, E. Schöll, and V. Anishchenko, Europhys. Lett. **112**, 40002 (2015).
[15] I. Omelchenko, A. Provata, J. Hizanidis, E. Schöll, and P. Hövel, Phys. Rev. E **91**, 022917 (2015).
[16] I. Omelchenko, O. E. Omelchenko, P. Hövel, and E. Schöll, Phys. Rev. Lett. **110**, 224101 (2013).
[17] S. A. Bogomolov, A. V. Slepnev, G. I. Strelkova, E. Schöll, and V. S. Anishchenko, Commun. Nonlinear Sci. Numer. Simul. **43**, 25–36 (2017).
[18] Y. Kuramoto and D. Battogtokh, Nonlinear Phenom. Complex Syst. **5**, 380 (2002).
[19] H. Sakaguchi and Y. Kuramoto, Prog. Theor. Phys. **76**, 576 (1986).
[20] E. A. Martens, S. Thutupalli, A. Fourriere, and O. Hallatschek, Proc. Natl. Acad. Sci. U.S.A. **110**, 10563 (2013).
[21] J. F. Totz, J. Rode, M. R. Tinsley, K. Showalter, and H. Engel, Nat. Phys. **14**, 282 (2018).
[22] M. S. Santos, J. D. Szezech, F. S. Borges, K. C. Iarosz, I. L. Caldas, A. M. Batista, R. L. Viana, and J. Kurths, Chaos Solitons Fractals **101**, 86 (2017).
[23] T. Kapitaniak, P. Kuzma, J. Wojewoda, K. Czolczynski, and Y. L. Maistrenko, Sci. Rep. **4**, 6379 (2014).
[24] N. Yao, Z.-G. Huang, C. Grebogi, and Y.-C. Lai, Sci. Rep. **5**, 12988 (2015).
[25] D. M. Abrams, R. Mirollo, S. H. Strogatz, and D. A. Wiley, Phys. Rev. Lett. **101**, 084103 (2008).
[26] S. I. Shima and Y. Kuramoto, Phys. Rev. E **69**, 036213 (2004).
[27] M. Wolfrum and O. E. Omelchenko, Phys. Rev. E **84**, 015201 (2011).
[28] C. R. Laing, Physica D **240**, 1960 (2011).
[29] G. Bordyugov, A. S. Pikovsky, and M. G. Rosenblum, Phys. Rev. E **82**, 035205 (2010).
[30] J. H. Sheeba, V. K. Chandrasekar, and M. Lakshmanan, Phys. Rev. E **81**, 046203 (2010).
[31] N. C. Rattenborg, C. J. Amlaner, and S. L. Lima, Neurosci. Biobehav. Rev. **24**, 817 (2000).
[32] G. Filatrella, A. H. Neilson, and N. F. Pedersen, Eur. Phys. J. B **61**, 485 (2008).
[33] E. Olbrich, J. C. Claussen, and P. Achermann, Philos. Trans. R. Soc. A **369**, 3884 (2011).
[34] Y. Kuramoto, D. Battogtokh, and H. Nakao, Phys. Rev. Lett. **81**, 3543 (1998).
[35] Y. Zhu, Z. Zheng, and J. Yang, Phys. Rev. E **89**, 022914 (2014).
[36] S. R. Ujjwal, N. Punetha, and R. Ramaswamy, Phys. Rev. E **93**, 012207 (2016).
[37] T. Banerjee, P. S. Dutta, A. Zakharova, and E. Schöll, Phys. Rev. E **94**, 032206 (2016).
[38] Y. Zhu, Y. Li, M. Zhang, and J. Yang, Europhys. Lett. **97**, 10009 (2012).
[39] Y. Suda, and K. Okuda, Phys. Rev. E **92**, 060901(R) (2015).
[40] Y. Kawamura, Phys. Rev. E **75**, 056204 (2007).
[41] I. A. Shepelev, G. I. Strelkova, and V. S. Anishchenko, Chaos **28**, 063119 (2018).
[42] G. Xiao, W. Liu, Y. Lan, and J. Xiao, Nonlinear Dyn. **93**, 1047 (2018).
[43] A. K. Malchow, I. Omelchenko, E. Schöll, and P. Hövel, Phys. Rev. E **98**, 012217 (2018); D. Dudkowski, Y. Maistrenko, and T. Kapitaniak, Phys. Rev. E **90**, 032920 (2014); D. Dudkowski, Y. Maistrenko, and T. Kapitaniak, Chaos **26**, 116306 (2016).
[44] O. E. Omelchenko, Y. L. Maistrenko, and P. A. Tass, Phys. Rev. Lett. **100**, 044105 (2008).
[45] A. Yeldesbay, A. Pikovsky, and M. Rosenblum, Phys. Rev. Lett. **112**, 144103 (2014).
[46] L. Schmidt and K. Krischer, Phys. Rev. Lett. **114**, 034101 (2015).
[47] V. K. Chandraasekar, R. Gopal, A. Venkatesan, and M. Lakshmanan, Phys. Rev. E **90**, 062913 (2014).
[48] T.-W. Ko and G. B. Ermentrout, Phys. Rev. E **78**, 016203 (2008).
[49] H. Wang and X. Li, Phys. Rev. E **83**, 066214 (2011).
[50] L. Schmidt, K. Schönleber, K. Krischer, and V. Garcia-Morales, Chaos **24**, 013102 (2014).
[51] G. C. Sethia and A. Sen, Phys. Rev. Lett. **112**, 144101 (2014).
[52] C. Meena, K. Murali, and S. Sinha, Int. J. Bifurc. Chaos **26**, 1630023 (2016).
[53] A. V. Cano and M. G. Cosenza, Chaos **28**, 113119 (2018).
[54] B. K. Bera, D. Ghosh, and M. Lakshmanan, Phys. Rev. E **93**, 012205 (2016).
[55] C. R. Laing, Phys. Rev. E **92**, 050904(R) (2015).
[56] B.-W. Li and H. Dierckx, Phys. Rev. E **93**, 020202 (2016).
[57] P. M. Gade, Phys. Rev. E **54**, 64 (1996).
[58] J. Jost and M. P. Joy, Phys. Rev. E **65**, 016201 (2002).
[59] F. M. Atay et al., Phys. Rev. Lett. **92**, 144101 (2004).
[60] P. M. Gade and C.-K. Hu, Phys. Rev. E **62**, 6409–6413 (2000).
[61] C. Li and G. Chen, Physica A **341**, 73 (2004).
[62] H. Aref, Annu. Rev. Fluid Mech. **15**, 345 (1983).
[63] A. Hilgers et al., Europhys. Lett. **45**, 552 (1999).
[64] R. J. Hendry and J. M. McGlade, J. Weiner Ecol. Modell. **84**, 81 (1996).
[65] S. Sinha and W. L. Ditto, Phys. Rev. Lett. **81**, 2156 (1998).
[66] S. Sinha and W. L. Ditto, Phys. Rev. E **60**, 363 (1999).
[67] S. Jalan and R. E. Amritkar, Phys. Rev. Lett. **90**, 014101 (2003).
[68] S. Jalan, R. E. Amritkar, and C.-K. Hu, Phys. Rev. E **72**, 016211 (2005).
[69] F. Ginelli, R. Livi, and A. Politi, J. Phys. A **35**, 499 (2002).
[70] M. Ding and W. Yang, Phys. Rev. E **56**, 4009 (1997).
[71] G. Robb and A. Politi, Phys. Rev. E **95**, 040201(R) (2017).

[72] J. Soriano, M. Rodriguez Martinez, T. Tlusty, and E. Moses, Proc. Natl. Acad. Sci. U.S.A. **105**, 13758 (2008).

[73] S. Luccioli, S. Olmi, A. Politi, and A. Torcini, Phys. Rev. Lett. **109**, 138103 (2012).

[74] C. Anteneodo, S. E. S. Pinto, A. M. Batista, and R. L. Viana, Phys. Rev. E **68**, 045202 (2003).

[75] C. Anteneodo, A. M. Batista, and R. L. Viana, Phys. Lett. A **326**, 227–233 (2004).

[76] J. P. Eckmann, S. O. Kamphorst, and D. Ruelle, Europhys. Lett. **5**, 973 (1987); M. S. Santos, J. D. Szezech, Jr., A. M. Batista, I. L. Caldas, R. L. Viana, and S. R. Lopes, Phys. Lett. A **379**, 2188–2192 (2015).

[77] N. Marwan, M. C. Romano, M. Thiel, and J. Kurths, Phys. Rep. **438**, 237–329 (2007); N. Marwan, C. L. Webber, E. N. Macau, and R. L. Viana, Chaos **28**, 085601 (2018).

[78] K. Kaneko, Chaos **25**, 097608 (2015).

[79] V. Santos, J. D. Szezech, A. M. Batista, K. C. Iarosz, M. S. Baptista, H. P. Ren, C. Grebogi, R. L. Viana, I. L. Caldas, Y. L. Maistrenko, and J. Kurths, Chaos **28**, 081105 (2018).

[80] F. P. Kemeth, S. W. Haugland, L. Schmidt, I. G. Kevrekidis, and K. Krischer, Chaos **26**, 094815 (2016).

[81] S. Majhi and D. Ghosh, Chaos **28**, 083113 (2018).

[82] M. E. J. Newman and D. J. Watts, Phys. Lett. A **263**, 341 (1999).

[83] D. Wu, S. Zhu, X. Luo, and L. Wu, Phys. Rev. E **84**, 021102 (2011).

[84] G. Pfurtscheller and C. Neuper, Neurosci. Lett. **174**, 93 (1994).

[85] C. M. Krause, H. Lang, M. Laine, and B. Pörnf, Electroencephalogr. Clin. Neurophysiol. **98**, 319 (1996).

[86] L. Leocani, C. Toro, P. Manganotti, P. Zhuang, and M. Hallet, Electroencephalogr. Clin. Neurophysiol. **104**, 199–206 (1997).